Investigation of Channel Vortices in Francis Turbines

M LIU[1], L J ZHOU[1], Z W WANG[2], D M LIU[3] and Y Z ZHAO [3]

[1] College of Water Conservancy and Civil Engineering, China Agriculture University, Beijing, China, 100083
[2] Department of Thermal Engineering, Tsinghua University, Beijing, China, 100084
[3] Research & Test Center Dongfang Electrical Machine, Dongfang Electrical Machinery Co., Ltd, Sichuan, China, 618000

E-mail: zlj@cau.edu.cn

Abstract. In this paper the characteristics of one type of channel vortex and the effect of different parameters on this channel vortex have been investigated experimentally with the aid of high speed photography. The results show that locations of the channel vortices move from near the hub down to near the band with the increase n_{11} or the decrease Q_{11}. Meanwhile, with the decrease of Q_{11} or σ, channel vortices become thicker with increasing appearing frequency. When the channel vortices come out near the hub or in the middle of the blade at low or moderate n_{11}, the main frequency of pressure pulsation in the draft tube is the swirling frequency of vortex rope. However when the channel vortices come out near the band at high n_{11}, the pressure pulsation in the draft tube has a wide-band spectrum with the frequency within 0.7~1f_n (rotating frequency). Then detailed numerical simulations were carried out to investigate the observed phenomenon. The results reveal this channel vortex is caused by the reversed flow in the draft tube. The mechanism is that channel vortices are induced when the reversed fluid flows up along the suction side of the blade and meets the upstream main flow.

1. Introduction

Huge Francis turbines are widely used in high head hydropower stations in recent years. The safe and stable operation has become a main concern for this kind of turbines. The cause of turbine operating instability is very complicated, including hydraulic factors, mechanical factors and electromagnetic factors. If the range of operating heads in a Francis turbine is extreme, the occurrence of inter blade vortex at partial load and high head may become unavoidable [1]. Meanwhile, the wrap angle and channel length of blade tend to be larger in order to improve the comprehensive performance of turbine, which makes the gather of vortices in inter-blade channels easier. In the past, there was an opinion that channel vortices were scattered in various flow channels and unlikely to form the resultant force. Thus, the threat of channel vortices to operating stability was small. But when channel vortices further develop, they may form a thick vortex rope which may cause vibration, noise and even blade crack. A lot of studies have been made to introduce the effect of channel vortices to the safe and stable operation of hydraulic turbine unit [2-4]. Escaler et al. [5] have provided that channel vortex is a very aggressive type of cavitation that is likely to deeply erode the blades and to provoke pressure fluctuations. Dörfler et al. [1] found that strong mechanical vibration may be caused by channel vortices because the wide-band excitation spectrum may excite the natural frequencies of many components of the turbine structure. To control the influence of channel vortices on the stable operation of Francis turbines, channel vortices experiments are required in more and more model

acceptance tests of the runner, especially for large units. Through these experiments the channel vortex inception line was drawn on the hill chart.

Researches on the inter-blade vortex flows have been focused on the predictions of the appearances of the vortices, the analysis of the characteristics and the induced pressure fluctuation [6-15], and the records of the temporal and spatial evolution of channel vortices [9, 16]. From these reported experimental studies, no conclusive frequency of the channel vortices was identified through the spectrum analysis of the results of pressure fluctuations due to its stochastic, wide-band nature [1]. However, it was indicated that the existence of the unstable channel vortices could induce alternating loads on the runner blades, which could result in a fatigue failure of them. On the other hand, most of numerical investigations were carried out through single-phase flow simulations under some special conditions and it was believed that the channel vortex under these conditions is caused by the high positive incident angle [10, 17]. However, channel vortices not only come out under high head part load conditions with high positive attack angle, but also appear under low head conditions with even negative attack angle. It suggests that the mechanism of the channel vortices and the influence factors are still not fully understood.

The main objective of this paper is to investigate the mechanism of channel vortices and effect of different parameters on them. The main concerns are put on the conditions on the channel vortex inception line. High speed photography was adopted to record the evolution of channel vortices. Results of different conditions were analyzed to find out the effect of unit speed n_{11}, unit flow rate Q_{11} and cavitation number σ on channel vortices. Pressure pulsation characteristics for these conditions were also presented. Finally, the reason for the observed channel vortices was analyzed based on the numerical simulation and experimental results.

2. Experimental Setup and Procedures

2.1. Experimental equipment

The model test rig is illustrated in Figure 1. The Francis turbine model used in experiment has a non-dimensional specific speed $n_s = 155.4$. The reduced model runner is 0.35m in diameter. The experiments were taken with the rotational speed of about 1000 r/min. To record the channel vortex in the Francis turbine, a high-speed photography system phantom V210 was used as shown in Figure 1, consisting of a high-speed camera, a lens, illuminating device, and computer components. The high-speed camera could record up to 2,000 frames/s but offered limited resolution of 1280 x 720 pixels. Considering the size of runner, the images were recorded at 1,000 frames/s with 1280 x 720-pixel resolution. Because of the memory limit of camera, a total of 4 seconds of movie was recorded, which meant that about total 4000 frames during about 60 rotations were recorded for each condition. A high-intensity xenon flash lamp was used as light source to illuminate the channel vortex obliquely from underside. There was a 45° angle between the lamp and the optical axes of the high-speed camera. The light from the lamp was focused on the outlet of blades through the draft tube cone which was made of plexiglass.

Pressure pulsations were measured in several points including the 4 points in the vaneless space, 2 points in draft tube as shown in Figure 1. Here DTCT means the measure points were in the Y direction in the cross section of $0.1D_2$ away from the inlet of draft tube cone. DTCH means the measure points were in the X direction in the cross section of $0.1D_2$ away from the inlet of draft tube cone. In the vaneless space 4 points were set with ±X located in the X direction, ±Y in the Y direction. An endoscope was also installed in the vaneless space to observe the cavitation behavior near the blade inlet.

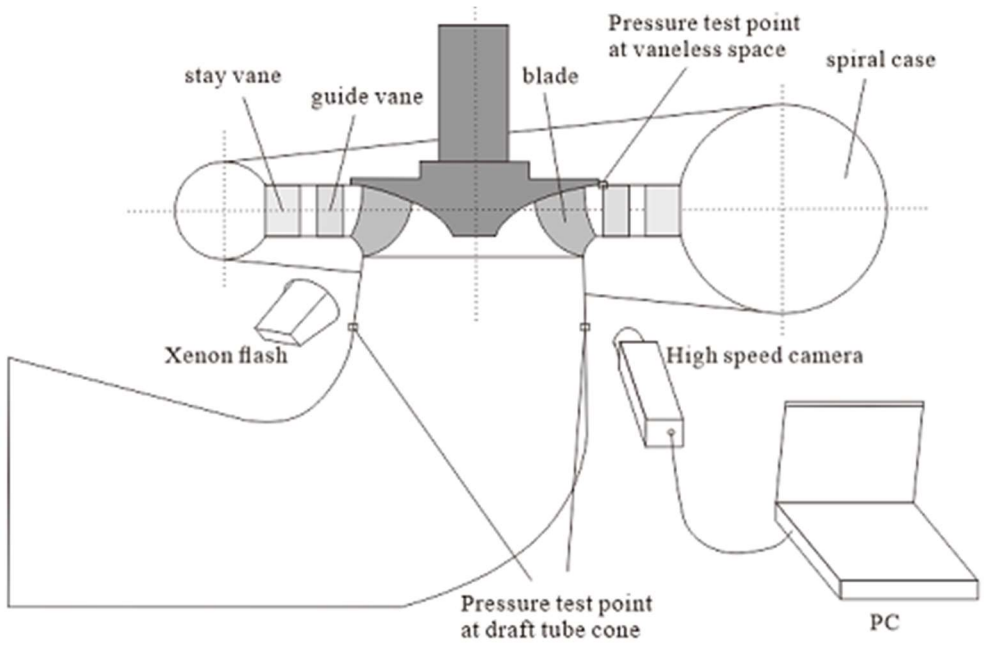

Figure 1. Schematic of experimental setup

2.2. Experimental equipment

Before the experiments, the channel vortex incipient line in the hill chart had already been drawn in the previous model test with the aid of synchronized stroboscope, as shown by the line with white block point in Figure 2.

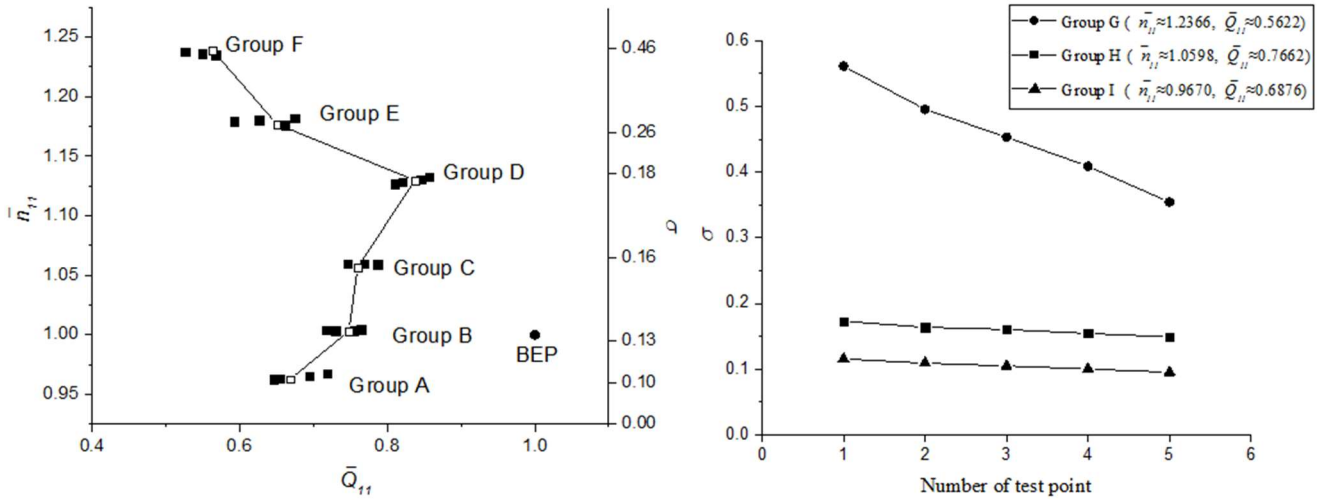

a) Conditions of normal channel vortex experiment b) Points of channel vortex experiment with different σ

Figure 2. Experimental conditions

The first experiment was carried out to investigate the influence of operation conditions on the channel vortex. Totally 6 groups of n_{11} were selected within the prototype operation range. For each n_{11}, the cavitation number (σ) was determined according to the tail water level of the prototype at the corresponding head. The pressure on the draft tube outlet was then set to meet the Cavitation number. About 5 openings were selected for each n_{11} including the channel vortex incipient point, 2 points on the left side (with less discharge) and 2 points on the right side (with larger discharge). Since the main concern of this paper was put on the conditions near the channel vortex incipient line, the opening variation for each n_{11} was limited in a relatively small range as shown in Figure 2. The experimental conditions in group A were named as A1, A2, A3, A4 and A5, with the discharge increasing

successively. The condition points in other groups were named in the same way. All the experimental points are shown in Figure 2. The $\bar{Q}_{11}$ and $\bar{n}_{11}$ in Figure 2 are unit discharge and unit speed normalized by the optimum point Q_{11o} and n_{11o}. The dot point marked as BEP is the optimum point normalized by itself.

The second experiment was to investigate the influence of cavitation number on the behavior of the channel vortex. In this experiment, totally 3 groups of points were selected as shown in Figure 3. In each group $\bar{Q}_{11}$ and $\bar{n}_{11}$ were almost identical. Five different cavitation number σ were selected for each group. The experimental conditions in group G were named as G1, G2, G3, G4 and G5 with the cavitation number decreasing successively. The same rule was used to name group H and I.

3. Experimental Results and Analyses

3.1. Effect of $\bar{n}_{11}$ on the behavior of channel vortices

In the first experiment, it was found that locations of channel vortices move from near the hub down to near the band with the increase of n_{11}. To save space, only pictures on the channel vortex incipient line (drawn in Figure 2 with white block points) are given in Figure 3 as an example. Each picture in Figure 3 shows one of the typical frames in the corresponding recorded movies.

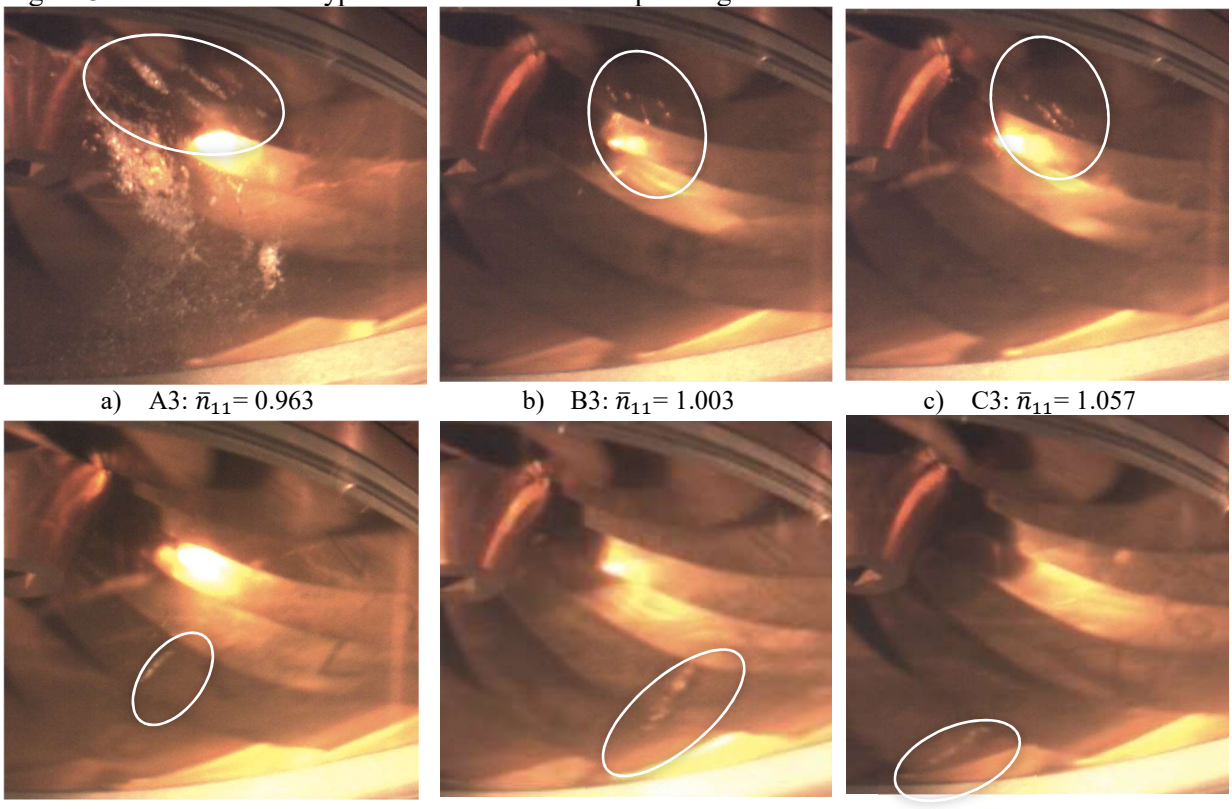

a) A3: $\bar{n}_{11}$= 0.963 b) B3: $\bar{n}_{11}$= 1.003 c) C3: $\bar{n}_{11}$= 1.057

d) D3: $\bar{n}_{11}$= 1.130 e) E3: $\bar{n}_{11}$= 1.177 f) F3: $\bar{n}_{11}$= 1.239

Figure 3. Photographs of channel vortices with different $\bar{n}_{11}$

The channel vortices are highlighted by white oval in these pictures. At low n_{11} conditions such as group A, B and C, the channel vortices came out from near the hub. When it moved to middle n_{11} conditions such as group D and E, the channel vortex could be seen swirling from the blade channel to the middle of the blade outlet. At the highest n_{11} condition group F, the channel vortices usually appeared near the band.

Moreover, for the conditions with low n_{11} such as conditions group A, B and C, the channel vortices came out from several neighbouring blade channel near the hub in certain periodic way. The period seemed to be related to the swirling vortex rope in the draft tube (see 3.5 in detail). However,

for the conditions with middle or high n_{11} (group E and F) the channel vortex only came out from some of the blade channels in a random way.

3.2. Effect of Q_{11} on channel vortices

Since the main concern of this paper was put on the conditions near the channel vortex inception line, the flow rate for each group of n_{11} varied within a relatively small range. However, the movies still show that Q_{11} has obvious influence on not only the appearance and location of the channel vortex but also its appearing frequency. For example, pictures for the conditions with $\bar{n}_{11} \approx 1.24$ and $\sigma \approx 0.46$ (group F, Figure 4) show that with the decrease of Q_{11}, channel vortices become thicker. And the channel vortex is intermittent when Q_{11} is large (F4). While it becomes continuous in low Q_{11} (F2 and F1). Moreover, the location of channel vortex slightly moves to near band with the decrease of Q_{11}. In order to present this phenomenon better, photographs for two other conditions ($\bar{n}_{11} \approx 1.18$ and $\sigma \approx 0.26$ in group E) with a bit larger difference in Q_{11} are shown in Figure 4d and Figure 4e. It is obvious that location of channel vortex moves to nearer the band with the decrease of Q_{11}.

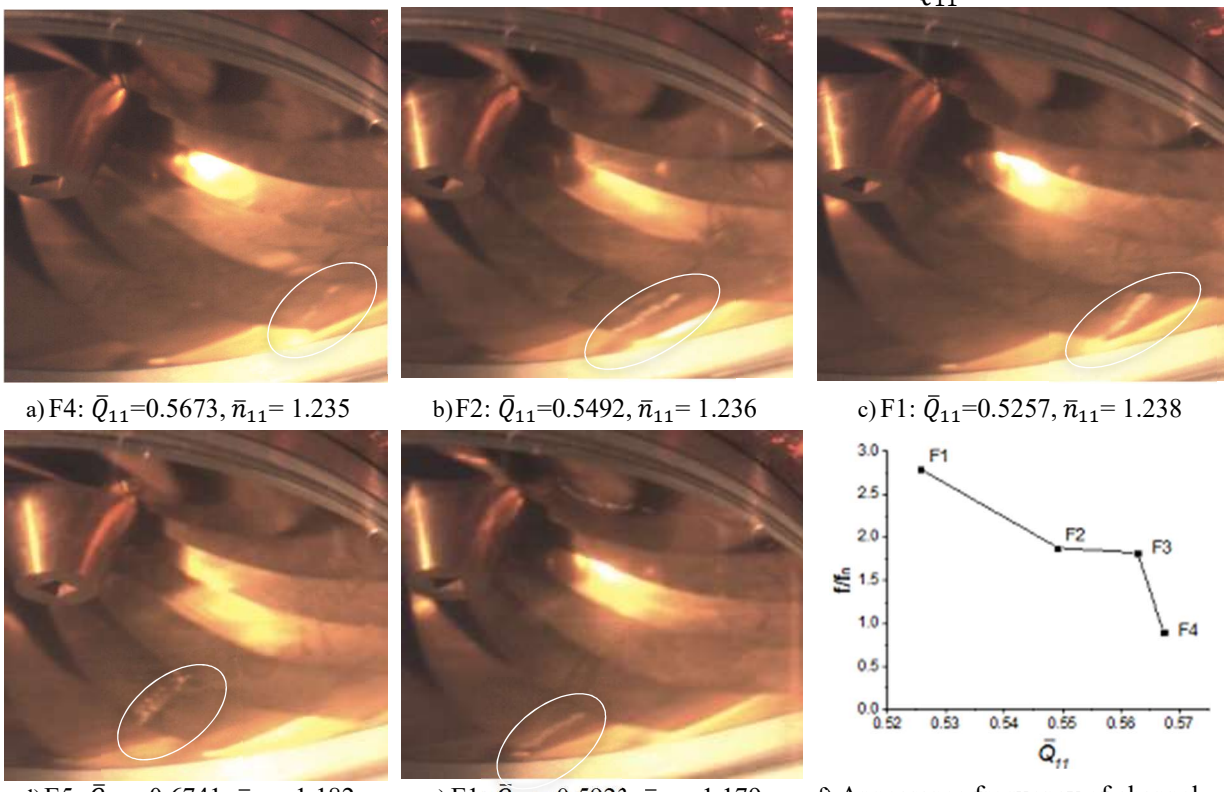

a) F4: $\bar{Q}_{11}$=0.5673, $\bar{n}_{11}$= 1.235 b) F2: $\bar{Q}_{11}$=0.5492, $\bar{n}_{11}$= 1.236 c) F1: $\bar{Q}_{11}$=0.5257, $\bar{n}_{11}$= 1.238

d) E5: $\bar{Q}_{11}$= 0.6741, $\bar{n}_{11}$= 1.182 e) E1: $\bar{Q}_{11}$= 0.5923, $\bar{n}_{11}$= 1.179 f) Appearance frequency of channel vortex of group F

Figure 4. Effect of $\bar{Q}_{11}$ on location of channel vortices

Moreover, for the conditions with middle or high n_{11}, more channel vortices appeared within 4 seconds of recording time with the decrease of the flow rate. Because the color of channel vortex is hard to distinguish from reflection illumination, it is very difficult to use intelligent image-recognition software to count the number of channel vortex. Besides, the experimental conditions are near the incipient point, and channel vortices come out in a random way for conditions group E, F and G. Thus, the number of channel vortices appearing during the total recording time was counted manually. Figure 4f gives the appearing frequency of the channel vortex. The value of Y axis is the appearance frequency of channel vortices divided by the rotational frequency of the runner. It indicates that the appearance frequency generally grows up with the decrease of Q_{11}.

3.3. Effect of cavitation number σ on channel vortices

Among the three groups of points in the second experiment, group H and I had relative low $\bar{n}_{11}$ and the vortex behavior at different cavitation numbers is similar. Thus, only pictures under group G and H are given here to show the effect of cavitation number σ on channel vortices.

Photographs recorded for conditions group G and H shown in Figure 5 indicate that with the decrease of σ, channel vortices show a trend of becoming thicker. The channel vortex is intermittent when σ is large, while it becomes continuous at small σ. Apart from that, one can also find that channel vortices arise from more blade channels with the decrease of σ. Figure 5c also shows the appearing frequency of channel vortex increase with the decrease of σ.

However, the pictures show that location of the channel vortex for each group was not affected by the cavitation number σ.

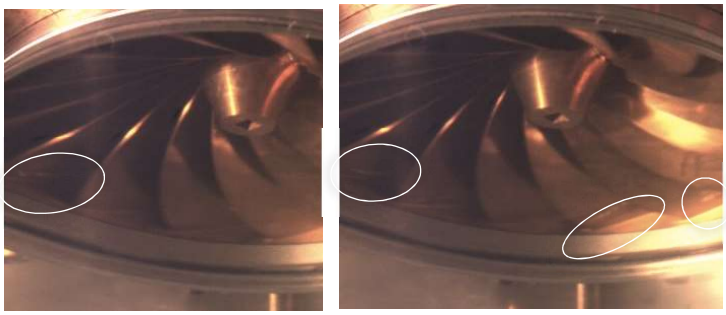

a) G1: σ=0.5609 b) G5: σ =0.3541

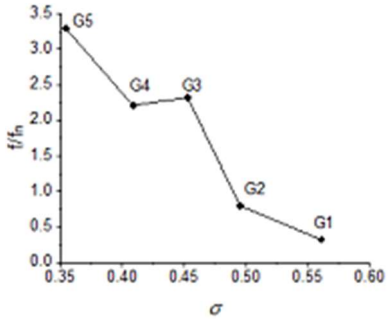

c) Appearance frequency of channel vortex of group G

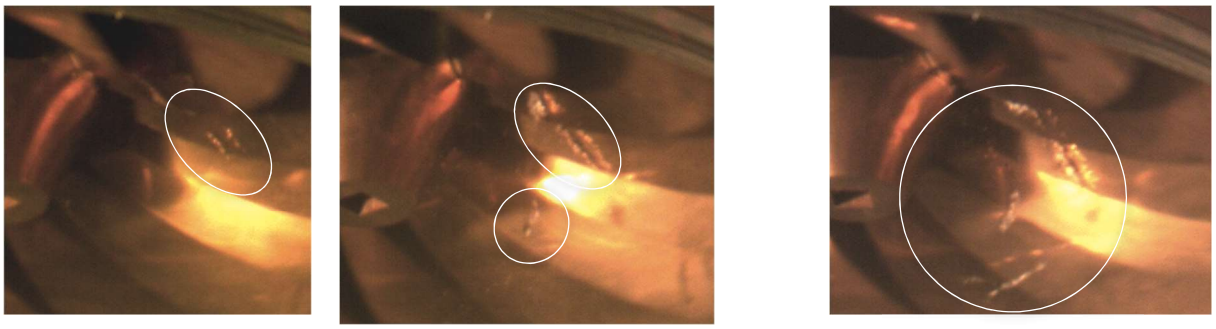

d) H1: σ=0.1726 e) H3: σ=0.1601 f) H5: σ=0.1489

Figure 5. Photographs of channel vortices with different σ of group G and H

3.4. Pressure pulsation characteristics under the conditions with channel vortex

The pressure pulsations on several points in the draft tube and vaneless space were recorded for all above conditions. The dominant frequency in the draft tube at low and middle n_{11} conditions (group A, B, C and D) is the typical swirling frequency of the vortex rope. Although there exist $0.5f_n$ and f_n components, the spectral peak of the precession frequency is dominant. However when the channel vortices come out near the band at high n_{11}, the pressure pulsation in the draft tube becomes a broadband pulsation. There is no obvious dominant frequency and its peak frequency is about $0.73f_n$. The first peak frequency in the draft tube is shown in Figure 6 for all conditions, in which the sharp peak is presented by the point, while the wide band peak is presented by the point in the rectangle. Figure 6 shows that for conditions E1 to E5 ($\bar{n}_{11} \approx 1.18$, $\sigma \approx 0.26$) the pick frequency increases with the decrease of Q_{11}. Similar phenomena were reported in Yamamoto's paper [15] which investigates the cavitation phenomena at deep part load condition and pressure fluctuations associated with the phenomena. For conditions F1 to F4, the first peak frequency remains in the range of $0.7\sim1f_n$.

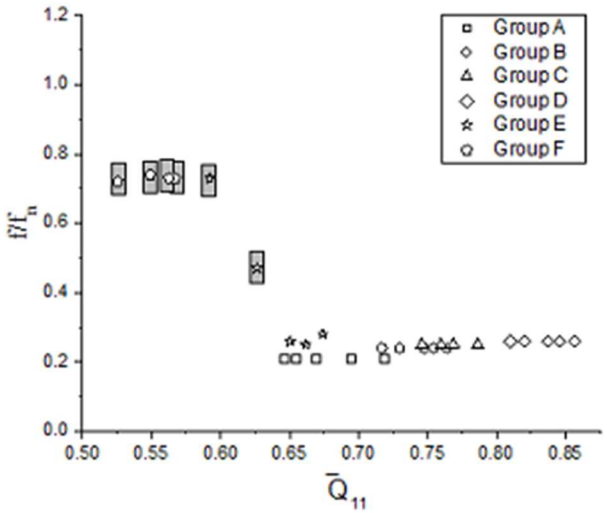

Figure 6. Pressure pulsation peak frequency at draft tube cone section for all conditions

In the spectrums in the vaneless space the blade passing frequency $15f_n$and rotation frequency f_n were two of the main frequencies for all conditions as expected. With the conditions in group A, B, C, D and conditions E1~E3, the 0.2~0.3f_n is also obvious except for another two peaks $15f_n$ and f_n, implying vortex rope swirling in the draft tube also affects the upstream pressure. While for other conditions there are only two peaks $15f_n$ and f_n.

3.5. The reversed flow near the hub

The observed channel vortices were obviously not caused by the high positive incident angle. Generally the head or n_{11} affects the incident angle more than the flow rate. At the high head (or low n_{11}) conditions the inlet attacking angle usually has the high positive value, while at the very low head (or high n_{11}) it has the negative value. But the observed channel vortices appeared not only at low n_{11} conditions, but also at high n_{11} conditions. Besides, no cavitation vortex was observed near the inlet by the endoscope for conditions group B, C, D, E and F, that means the vortices come out from the outlet was not related to the high positive incident angle. Besides, above results was also found in a number of other model tests with different Francis runner, which implies that the above observation is the common case for some runners other than a single special case. It suggests that the channel vortex observed in these model tests are caused by the same mechanism.

It is very interesting to notice that for conditions A1 to A5, the appearing of channel vortices were always accompanied by the vortex rope in the draft tube. And the position of the channel vortices in the runner moved with the swirling period of the vortex rope. It is well know that at the part load condition there exists reversed flow in the center part of the draft tube [18-21].

For other conditions with low to moderate $\bar{n}_{11}$ (group B, C and D), although vortex rope was not visible in the recorded photographs, the pressure fluctuation in the draft tube show clearly the typical feature of the vortex rope. In fact, when the cavitation number σ decreases to a certain degree, vortex rope would be visible under these conditions. Experiments also showed that the pressure fluctuation in the draft tube for conditions E5 has the typical feature of the vortex rope. But when the flow rate decreased, the pressure pulsation in the draft tube began to show a wide-band spectrum with the peak frequency increase (See Figure 6c, conditions E5 to condition E1). Yamamoto's work [15] presented the same tendency and their experiments showed that at part load condition with the decrease of the flow rate, the vortex rope disappeared. Instead, a large stagnation region existed in the middle of the draft tube, which meant that the area of the inversed flow increased. On the other hand, in the case of high $\bar{n}_{11}$ conditions (group F), the pressure pulsations in the draft tube also had a wide-band spectrum with the peak frequency within 0.7~1f_n. This is also the typical spectrum when a large area of inversed flow appears in the draft tube.

In summary, the experimental results show that for all conditions when the channel vortices come out into view form the runner outlet, there is reversed flow in the center of the runner. The reversed flow in the draft tube flowing back to the runner was reported by Côté et al. [19] in their work investigating the flow behavior in a Francis runner during load rejection, referred as the pumping phenomenon. However, it was not linked to the channel vortex. Is the channel vortex related to this reversed flow? In order to answer this question, numerical simulations were conducted for several runners. The readers can refer to another paper [22] for the detailed description of the numerical method and the results. Here only the results on condition D3 are present as an example to explained the mechanism.

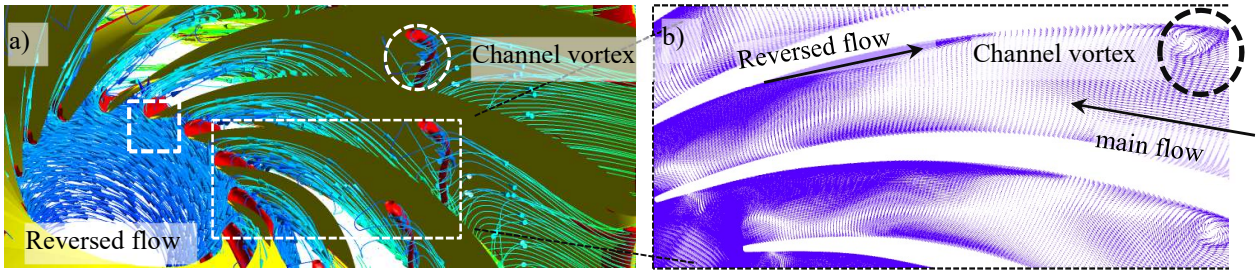

Figure 7. Streamlines inside the runner (up) and velocity vectors on the surface at 0.05 span (down)

The streamlines in the middle of the runner (Figure 7a) show the reversed flow hits the suction side of the blade near the trailing edge with large incident angle and results in two areas with $\lambda_2 < -2e^5$ highlighted by the square and the circle. The area in the square is caused by flow separation on the pressure side because of the large incident angle. However, the streamlines in this area do describe a closed or spiral path. The vortex in the circle is a secondary vortex that forms after part of the fluid flows back into the runner and causes the upstream main flow to separate from the blade suction side. The streamlines inside the vortex swirl in a spiral path. The velocity vectors on the surface at 0.05 span near the runner hub (Figure 7b) show the formation of this vortices in details.

3.6. The mechanism of the channel vortex

At this point, it is reasonable to conclude that the channel vortices observed in the experiments is caused by the reversed flow in the draft tube under part load conditions. And this mechanism is illustrated in Figure 8 schematically.

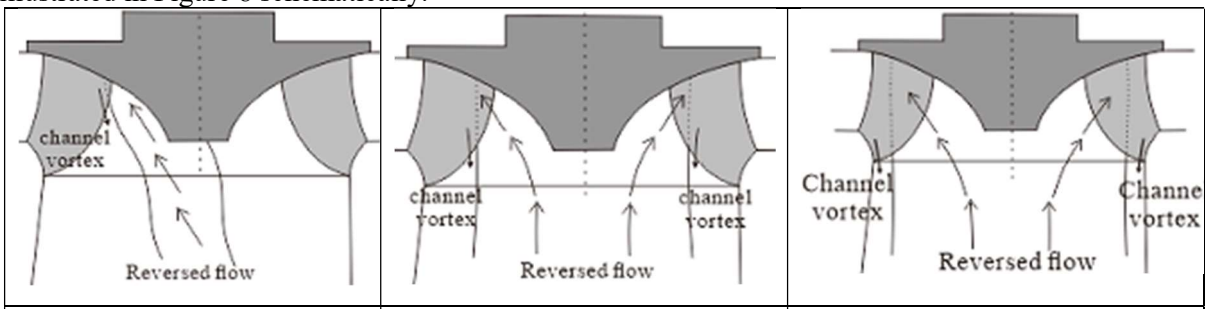

a) ConditionA3,B3, C3	c) Condition D3 & E3	c) Condition F3

Figure 8. The mechanism of the channel vortices observed in Figure 3

It is well known that there is reversed flow in the draft tube under part load conditions. And the reversed flow area on the blade suction side increases with the increase of n_{11} or decrease of Q_{11}, which pushes the channel vortex to move towards the inlet. Thus, if observing from the runner outlet, the channel vortex moves from hub to the band with the increase of n_{11} or decrease of Q_{11}, just as shown in Figure 3.

Meanwhile, when the reversed flow area is limited in a relatively small region, the vortex rope appears, the flow field in the draft tube is not symmetric with the reversed flow area swirling with a the same frequency of about 0.2~0.5f_n [19]. This explains Figure 7 which shows the channel vortex

comes out from several adjacent channels and the position of the channel vortices move with the swirling period of the vortex rope.

With the increase of n_{11}, the area of the inversed flow increases so that inter-blade channels are expected to be affected. However, the channel vortices are visible through the transparent draft tube because cavitation occurs in the vortex cores and they have obvious gas-liquid two phase feature. The visibility of the channel vortex depends greatly on the cavitation number. Considering that in the experiments the pressure at the draft tube outlet and cavitation number increased with the increase of n_{11} (because the tail water level of the prototype was high when the head was low, see Figure 2), it is easy to understand that the possibility of cavitation would be less at high n_{11}. This explains the phenomenon that the channel vortex comes out from only some of the blade channels in a random way for the conditions with middle or high n_{11} (group E and F).

On the other hand, if n_{11} keeps constant, the decrease of Q_{11} increases the area of the reversed flow and the magnitude of velocity. Thus, the vorticity of the channel vortex increases and the pressure inside the core decreases, which gives rise to the possibility of cavitation in the vortex. As a result, channel vortices become thicker and come out more frequently with the decrease of Q_{11} (see Figure 4).

Finally, with the decrease of σ, the overall pressure in the inter-blade channels reduced, which would make more cavitation vortex visible. Therefore, channel vortices appeared more frequently and became thicker, as observed in Figure 5.

4. Conclusion

In this study, the characteristics of one type of channel vortex and effect of different parameters on this channel vortex were investigated experimentally. The experimental results show that the location of channel vortices moves from near the hub down to near the band with the increase n_{11} or the decrease Q_{11}. Meanwhile, with the decrease of Q_{11} or σ, channel vortices become thicker with increasing appearing frequency. When the channel vortices come out near the hub or in the middle of the blade at low or moderate n_{11}, the main frequency of pressure pulsation in the draft tube is the swirling frequency of vortex rope. However, when the channel vortices come out near the band at high n_{11}, the pressure pulsation in the draft tube has a wide-band spectrum with the frequency within 0.7~1f_n.

Then detailed numerical simulations were carried out to investigate the mechanism of this type of channel vortex observed in experiments. The locations of the predicted vortices under different conditions agree well with experimental observation. The results reveal the mechanism of this type of channel vortex that the reversed fluid flows up along the suction side of the blade and induces channel vortices when it meets the upstream main flow.

5. Acknowledgments

The authors gratefully acknowledge the support from the National Natural Science Foundation of China (No. 51279205) and the Open Research Funded Project of Key Laboratory of Fluid Machinery in Sichuan Province (Xihua University) (Grant No. Szjj2012-041).

6. Nomenclature

D	runner diameter (m)	H_{st}	suction head (m)
g	the gravity acceleration(m/s^2)	p_{sat}	saturated vapor pressure (Pa)
H	operating head (m)	ρ	density (kg·m^{-3})
n	rotational speed (r/min)	σ	Cavitation number $\sigma = (p_{dt} - H_{st} - p_{sat}/\rho g)/H$
n_{11}	unit speed $n_{11} = (nD)/\sqrt{H}$	n_{11o}	unit speed at the optimum point
Q	flow rate (m^3/s)	Q_{11o}	unit discharge at the optimum point
Q_{11}	unit flow rate $Q_{11} = Q/(D^2\sqrt{H})$	$\bar{n}_{11}$	non-dimensional unit speed $\bar{n}_{11} = n_{11}/\sqrt{n_{11o}}$
n_s	non-dimensional specific speed	$\bar{Q}_{11}$	non-dimensional unit discharge

$n_s = 3.13\, n\sqrt{Q\eta}/H^{3/4}$ $\bar{Q}_{11} = Q_{11}/\sqrt{Q_{11o}}$

p_{dt} pressure on the draft tube outlet (Pa) η efficiency

References

[1] Dörfler P, Sick M and Coutu A 2012 *Springer Science & Business Media*
[2] Avellan F 2004 *Proc. 6th Int. Conf. on hydraulic machinery and hydrodynamics* (Timisoara: Romania)
[3] Kumar P and Saini R P 2010 *Renewable Sustainable Energy Rev* **14**(1) 374-383
[4] Guo T, Zhang L X, Wang W Q and Luo Z M 2014 *Advances in Mechanical Engineering* **6** 570189
[5] Escaler X, Egusquiza E, Farhat M, Avellan F and Coussirat M 2006 *Mech Syst Signal Process* **20**(4) 983-1007
[6] Xiao Y, Wang Z, Yan Z, Luo Y, Xiao R, Peng G and Xue P 2008 *Proc. ASME Fluids Eng. Div. Summer Conf., FEDSM* pp 1179-85
[7] Xiao Y, Wang Z, Zhang J, Peng G, Liu D, Ma X and Xiao M 2009 *Proc. ASME Fluids Eng. Div. Summer Conf., FEDSM* pp 1623-28
[8] Kurosawa S, Lim S and Enomoto Y 2010 *IOP Conf. Ser. Earth Environ. Sci.* **12**(1) 012063
[9] Song W, Wang H and Li J 2011 *Int. Conf. Consum. Electron., Commun. Networks, CECNet - Proc.* pp 4392-96
[10] Xiao Y, Wang Z and Yan Z 2011 *Eng. Comput. (Swansea Wales)* **28**(2) 154-171
[11] Yang Y, Wang H, Gong R, Wei X and Liu W 2011 *Proc. Int. Conf. Electron. Mech. Eng. Inf. Technol., EMEIT* pp 1675-78
[12] Flores E, Bornard L, Tomas L, Liu J and Couston M 2012 *IOP Conf. Ser. Earth Environ. Sci.* **15**(2) 022023
[13] Zhang H and Zhang L 2013 *Appl. Mech. Mater.* **291** pp 1958-62
[14] Magnoli M and Maiwald M 2014 *IOP Conf. Ser. Earth Environ. Sci.* **22**(3) 032013
[15] Yamamoto K, Müller A, Favrel A, Landry C and Avellan F 2014 *IOP Conf. Ser. Earth Environ. Sci.* **22**(2) 022011
[16] Aeschlimann V, Beaulieu S, Houde S, Ciocan G D and Deschenes C 2013 *Eur J Mech B Fluids* **42** 121-128
[17] Zuo Z, Liu S, Liu D, Qin D and Wu Y 2013 *Advances in Mechanical Engineering* **5** 397583
[18] Wang Z and Zhou L 2006 *J Fluids Eng Trans ASME* **128**(4) 649-655
[19] Côté P, Dumas G, Moisan É and Boutet-Blais G 2014 *IOP Conf. Ser. Earth Environ. Sci.* **22**(3) 032023
[20] Amiri K, Mulu B and Cervantes M J 2016 *J Fluids Eng Trans ASME* **138**(2) 021106
[21] Foroutan H and Yavuzkurt S 2015 *J Fluids Eng Trans ASME* **137**(6) 061101
[22] Zhou L, Liu M, Wang Z, Liu D and Zhao Y 2016 *Eng. Comput.* accepted